Multiple-Scale Turbulence and Bifurcation

M. Yagi 1), S.-I. Itoh 1), M. Kawasaki 1), K. Itoh 2), A. Fukuyama 3)

1) Research Institute for Applied Mechanics, Kyushu University, Kasuga, Japan
2) National Institute for Fusion Science, Toki, Japan
3) Department of Nuclear Engineering, Kyoto University, Kyoto, Japan

e-mail contact of main author: yagi@riam.kyushu-u.ac.jp

Abstract. In this paper, we analyze the turbulence composed of collective modes with different scale lengths. The hierarchical model for multiple-scale turbulence is developed. Nonlinear interactions between different scale length are modeled as turbulent drag, nonlinear noise and nonlinear drive and a set of Langevin equations is formulated. Using this model, a case where two driving mechanisms coexist (one for the micro mode and the other for semi-micro mode) is investigated. It is found that a new type of turbulence transition and a cusp-type catastrophe exist in some parameter regime. Numerical simulations are also performed for neighboring multiple-scale turbulence such as ion temperature gradient driven drift wave(ITG) ($k_y\rho_i < 1$) and short wavelength ITG($k_y\rho_i > 1$) modes in the shearless slab geometry. The cascade and inverse cascade in multiple-scale turbulence is investigated. The cascade is mainly observed in $k_{//}$ space. On the other hand, the cascade and the inverse cascade is observed in $k_\perp$ space. Another interesting result is that the particle flux is negative (inward pinch) due to the short wavelength ITG modes, while the ion and electron heat flux are positive, which indicates nonlinear interaction between different scale length mode might affect transport.

1. Introduction

Fluctuations with different scale lengths coexist in high temperature plasmas. In a conventional approach, the scale separation is assumed and one class of mode is analyzed neglecting fluctuations with other scale length. However, this simplification is not always relevant. For example, the dynamics of the meso-scale structure of the radial electric field is known to cause variation in the dynamics of microscopic fluctuations[1]. The interaction between zonal flow and drift wave turbulence is another example[2].

In this paper, we analyze the turbulence composed of collective modes with different scale lengths based on two approaches. First, the hierarchical model for multiple-scale turbulence is developed. Nonlinear interactions between different scale length are modeled as turbulent drag, nonlinear noise and nonlinear drive and a set of Langevin equations is formulated. Using this model, a case where two driving mechanisms coexist is investigated, where the drift-type fluctuations in the range of $k_y\rho_i \sim 1$ (ion temperature gradient driven drift wave(ITG), trapped particle modes, etc.) are called the 'semi-micro mode' and .those in the range of $k_y c/\omega_{pe} \sim 1$ are called the 'micro mode'. It is found that a new type of turbulence transition and a cusp-type catastrophe exist. A new insight is given for the physics of the internal transport barrier. Next, numerical simulations are also performed for neighboring multiple-scale turbulence such as ITG($k_y\rho_i < 1$) and short wavelength ITG($k_y\rho_i > 1$) modes[3] in the shearless slab geometry. The cascade and inverse cascade in multiple-scale turbulence is investigated. The cascade is mainly observed in $k_{//}$ space. On the other hand, the cascade and the inverse cascade is observed in $k_\perp$ space. Another interesting result is that the particle flux is negative (inward pinch) due to the short wavelength ITG modes, while the ion and electron heat flux are positive. This result indicates nonlinear interaction between different scale length mode might affect transport. In
§2, the hierarchical model is discussed. Nonlinear simulation is explained in §3.

2. Nonlinear Interplay and Transition in Multiple-Scale Turbulence

2.1 Transition in Multiple-Scale Turbulence

To derive the hierarchical model for multiple-scale turbulence, the effect of the semi-micro mode to the micro mode is taken into account. The local pressure steepening and the **E**x**B** shearing induced by semi-micro fluctuations are incorporated into the model. The former has the destabilizing influence and the latter has suppressing effect on micro mode. The change of local magnetic shear by the semi-micro mode is not kept in this model, since the semi-micro mode is assumed to be electrostatic mode. ITG mode and current diffusive interchange mode (CDIM)[4] are considered as semi-micro and micro modes, respectively. A detailed derivation of the Langevin equation and the deduction of the statistical average are explained in [5]. Langevin equations for semi-micro mode and micro mode are given by

$$\frac{dx_l}{d(\omega_l t)} + \frac{1}{2}\left(\frac{\sqrt{x_h}}{r} + \sqrt{\frac{x_h}{r^2} + 4x_l} - 2\right)x_l - \frac{\varepsilon}{r^3}x_h^{3/2} + \frac{1}{2}\left(\frac{\sqrt{x_h}}{r} + \sqrt{\frac{x_h}{r^2} + 4x_l}\right)x_l w_l + \frac{\varepsilon}{r^3}x_h^{3/2} w_h = 0 \qquad (1)$$

$$\frac{dx_h}{d(\omega_h t)} + \left[\sqrt{x_h} - \sqrt{1 + \frac{\sqrt{x_l}}{\sqrt{x_h}/r + \sqrt{x_h/r^2 + 4x_l}}}\;/\,(1 + pr^2 x_l)\right]x_h - x_h^{3/2} w_h + \varepsilon^{1/2} w_l = 0 \qquad (2)$$

where superscripts l and h denote the semi-micro and micro modes[4]. $x_l = I_l / D_l^2$ and $x_h = I_h / D_h^2$ denote the spectral intensities of semi-macro mode, $I_l = \sum_{k_l} \left\langle \phi_{k_l}^* \phi_{k_l} \right\rangle$ and micro mode, $I_h = \sum_{k_h} \left\langle \phi_{k_h}^* \phi_{k_h} \right\rangle$ normalized by driving sources, D_l, D_h , which are defined by $D_l = \frac{2}{2 - C_l}\frac{\gamma_l}{k_l^2}\frac{1}{1 + \left(\omega_{E0} / \omega_{Ec}^l\right)^2}$ and $D_h = \frac{2}{2 - C_h}\frac{\gamma_h}{k_h^2}\frac{1}{1 + \left(\omega_{E0} / \omega_{Ec}^h\right)^2}$. $\gamma_{l,h}$ and $k_{l,h}$ are the maximum growth rate and corresponding wave number, $C_{l,h}$, numerical coefficients of order unity, ω_{E0} , the equilibrium electric field shear, $\omega_{Ec}^{l,h}$, the critical value of the inhomogeneous radial electric field for the suppression of modes. Explicit expressions of these valuables for ITG and CDIM are given in [3]. $\omega_{l,h} = k_{l.h}^2 D_{l,k} \sim \gamma_{l,k}$ represents typical growth rate for these modes and w_l, w_h, w_t are Gaussian white noise with mean zero and deviation unity. Other parameters are given by $r = D_l / D_h$ (the driving ratio of semi-micro and micro modes), $\varepsilon = \frac{C_h}{2 - C_l}(k_l / k_h)^2$ (the coupling coefficient for the drive of the semi-micro mode by the nonlinear noise of the micro mode) and $p = D_h^2 / I_{eff}$ with $I_{eff} = (1 + (\omega_{E0} / \omega_{Ec}^h)^2)(\omega_{Ec}^h)^2 / k_l^4$.

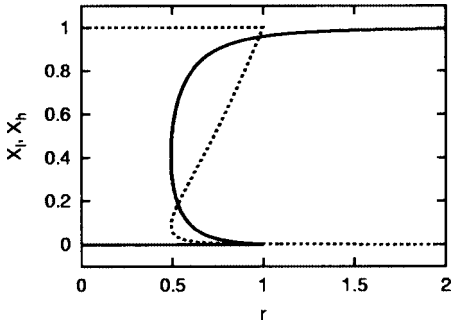

FIG.1 The steady state solution of eqs.(1) and (2) without noise term.

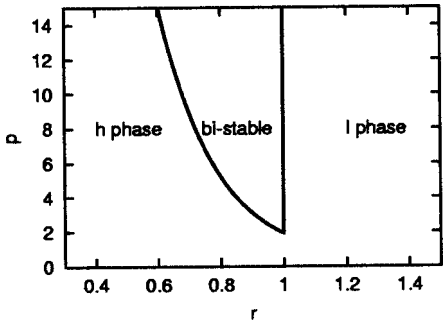

FIG.2 The phase diagram in (r,p) phase space.

Figure 1 shows the steady state solution of eqs. (1) and (2) without noise terms as a function of the driving ratio r . Parameters $p = 30$ and $\varepsilon = 0$ are used. The solid curve corresponds to the

semi-micro mode and the dashed curve to the micro mode. For $r < 0.493$, the micro mode is excited but the semi-micro mode is quenched. In the region $0.493 < r < 1$, the semi-micro mode is also excited and a hysteresis appears in the relation between the gradient and fluctuation level . For $1 < r$, the micro mode is quenched and only the semi-micro mode survives. The presence of hard bifurcation in the fluctuation level forms a cusp-type catastrophe in the phase space. Figure 2 shows the phase diagram with a cusp-type catastrophe in (r,p) phase space. In this diagram, the semi-micro mode is quenched in the region 'h phase' and the micro mode is quenched in the region 'l phase'. Both modes coexist in the region 'bi-stable'. If the trajectory cross over the region 'bi-stable' from 'l phase' (corresponding to L-mode state) to 'h phase' (corresponding to ITB state), then the hard transition will occur. Since $\sqrt{I_{l,h}}$ corresponds to the transport coefficient, this figure represents the cusp-type catastrophe of the turbulent transport.

2.2 Noise Effect on Multiple-Scale Turbulence

To investigate the noise effect on multiple-scale turbulence, the Fokker-Planck equation is derived for the semi-macro mode. Using the adiabatic approximation for the micro mode, it is given by

$$\frac{\partial P(x_l,t)}{\partial(\omega_l t)} = \frac{1}{2}\frac{\partial}{\partial x_l}\left(\frac{\sqrt{x_h^*}}{r} + \sqrt{\frac{x_h^*}{r^2} + 4x_l} - 2\right)x_l P(x_l,t)$$
$$+ \frac{1}{2}\frac{\partial^2}{\partial^2 x_l^2}\left[\frac{1}{4}\left(\frac{\sqrt{x_h^*}}{r} + \sqrt{\frac{x_h^*}{r^2} + 4x_l}\right)^2 x_l^2 + \frac{\varepsilon^2}{r^6}x_h^{*3}\right]P(x_l,t) \ , \qquad (3)$$

with

$$\sqrt{1 + \frac{\sqrt{x_l}}{\sqrt{x_h^*}/r + \sqrt{x_h^*/r^2 + 4x_l}}} \ / (1 + pr^2 x_l) - \sqrt{x_h^*} - \frac{3}{2}x_h^* = 0 \ , \qquad (4)$$

where eq.(4) is obtained from the maximum value of the steady state distribution function of the micro mode and the third term represents the noise effect from the micro mode[6].

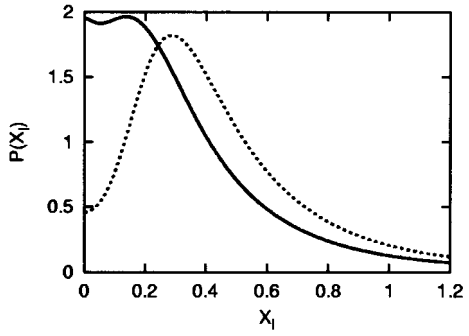

FIG.3 The steady state distribution function of the semi-micro mode.

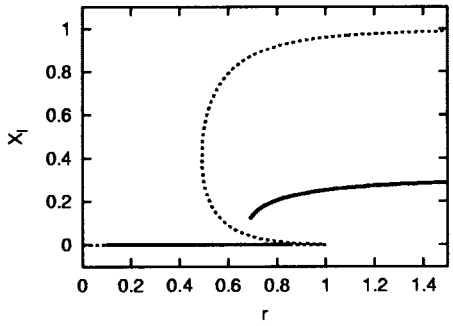

FIG.4 The most probable state for x_l as a function of r .

Figure 3 shows the steady state distribution function of the semi-micro mode. The solid curve represents the case with $r = 0.7, p = 30$ and the dashed curve represents the case with $r = 1.5, p = 30$. In the case with $r = 0.7$, Two peaks are observed, however, the well between two peaks is very shallow, which is due to the noise effect. Figure 4 shows the most probable

state for x_l as a function of r. The results from deterministic model are also shown by the dashed curve. It is found that for $r > 1$, the most probable state does not tend to unity. In that sense, we might say that the noise effect change the phase diagram drastically. For $r \sim 0.5$, there is a bi-stable region, however, the difference between two solutions is smaller than that from the deterministic model. The noise effect smears out the sharp boundary.

3. Cascade and Inverse Cascade in Multiple-Scale Turbulence

3.1 Model System of Direct Nonlinear Simulation

The numerical simulation is performed to investigate the cascade and inverse cascade in multiple-scale turbulence. We consider the neighboring turbulence such as ITG and the short wavelength ITG mode. The kinetic-fluid equations for the ion density n_k and the electrostatic potential ϕ_k, which are relevant to describe ITG and the short wavelength ITG mode in the shearless slab geometry are given by

$$\frac{\partial n_k}{\partial t} - i\omega_* \zeta_i Z_i \Gamma_{0k} \phi_k + \tau (1 + \zeta_i Z_i \Gamma_{0k}) \frac{\partial \phi_k}{\partial t} - i\eta_i \omega_* \Gamma_{0k} \zeta_i (\zeta_i + \zeta_i^2 Z_i - Z_i / 2) \phi_k$$
$$- i\eta_i \omega_* \zeta_i Z_i b_i (\Gamma_{0k} - \Gamma_{1k}) \phi_k + \frac{\tau}{2} \sum_{\mathbf{k} = \mathbf{k}' + \mathbf{k}''} \mathbf{z} \cdot \mathbf{k}'' \times \mathbf{k}' \Theta_{k''} \phi_{k'} = 0 \ , \tag{5}$$

$$\frac{\partial n_k}{\partial t} - i\omega_* \zeta_e Z_e \phi_k - (1 + \zeta_e Z_e + \lambda^2 k^2) \frac{\partial \phi_k}{\partial t} - i\eta_e \omega_* \zeta_e (\zeta_e + \zeta_e^2 Z_e - Z_e / 2) \phi_k$$
$$+ \frac{\tau}{2} \sum_{\mathbf{k} = \mathbf{k}' + \mathbf{k}''} \mathbf{z} \cdot \mathbf{k}'' \times \mathbf{k}' \phi_{k'} (n_{k''} - \lambda^2 k''^2 \phi_{k''}) = 0 \ , \tag{6}$$

with

$$\Theta_k = \chi_k (n_k + \tau \phi_k) + \eta_i \frac{\omega_*}{\omega} \zeta_i Z_i \left[(1 - b_i) \Gamma_{0k} + b_i \Gamma_{1k} \right] (\chi_k - \sigma_k) \tau \phi_k \ ,$$

$$\chi_{k''} = \frac{2}{\Gamma_{k''}} \int_0^\infty dx \, x e^{-x^2} dx J_0(kx) J_0(k'x) J_0(k''x) \ ,$$

$$\sigma_{k''} = \frac{2}{(1 - b_i'') \Gamma_{0k''} + b_i'' \Gamma_{1k''}} \int_0^\infty dx \, x^3 e^{-x^2} dx J_0(kx) J_0(k'x) J_0(k''x) \ ,$$

where the linear gyrokinetic response is used as a closure for equations and the ion gyro frequency Ω_i and ion Lamor radius ρ_i are used for normalizations[7]. $Z_{i,e}$ is the plasma dispersion function with the argument $\zeta_{i,e} = \omega / (k_{//} v_{thi,the})$, $\Gamma_{0k,1k} = I_{0,1}(b_i) e^{-b_i}$ with $b_i = k_\perp^2 \rho_i^2 / 2$ and $\lambda^2 = (\Omega_i^2 / \omega_{pi}^2) \tau / 2$ with $\tau = T_e / T_i$ [8]. In the limit of $\eta_e = \eta_i = 0$ and $1 << \zeta_i, \zeta_e << 1$ for $k_{//} \neq 0$, the energy conservation relation is written as

$$\frac{\mathrm{d}}{\mathrm{d}t} \left\{ \sum_{k_{//} \neq 0} \left[1 + k^2 \lambda^2 + \tau (1 - \Gamma_{0k}) \right] \left| \phi_k \right|^2 + \sum_{k_{//} = 0} \left[k^2 \lambda^2 + \tau (1 - \Gamma_{0k}) \right] \left| \phi_k \right|^2 \right\} = 0 \ , \tag{7}$$

where the first term in the left hand side represents the drift wave energy and the second term the convective cell energy. 1D and 2D energy spectra of the potential energy and flux are defined by

$$E_\phi(k_{//}) = \sum_{k_x, k_y} \left| \phi_k \right|^2, \ E_\phi(k_x, k_y) = \sum_{k_{//}} \left| \phi_k \right|^2 \tag{8}$$

$$\Gamma_{nk} = -i \sum_{\mathbf{k} = \mathbf{k}' + \mathbf{k}''} \frac{\tau}{2} n_k k_y' \phi_{k'}, \ q_{ik} = -i \sum_{\mathbf{k} = \mathbf{k}' + \mathbf{k}''} \frac{\tau}{2} p_{ik} k_y' \phi_{k'}, \ q_{ek} = -i \sum_{\mathbf{k} = \mathbf{k}' + \mathbf{k}''} \frac{\tau}{2} p_{ek} k_y' \phi_{k'} \tag{9}$$

where the ion and electron pressure are evaluated by using the linear distribution function such as $p_{ik,ek} = m_{i,e} / 3 \int d^3v\, v^2 f^{lin}_{ik,ek}$, then $p_{ik} = (-\tau + K / 3)\phi_k$ and $p_{ek} = \tau\,(1 + L / 3)\phi_k$ with

$K = -2\zeta_i(\tau + \omega_* / \omega)[Z_i\{(1 - b_i)\Gamma_{0k} + b_i\Gamma_{1k}\} + \zeta_i(1 + \zeta_i Z_i)\Gamma_{0k}]$

$+ \eta_i \omega_* / \omega \zeta_i[3Z_i\{(1 - b_i)\Gamma_{0k} + b_i\Gamma_{1k}\} - 4\zeta_i(1 + \zeta_i Z_i)(\{(1 - b_i)\Gamma_{0k} + b_i\Gamma_{1k}\}$

$- 4Z_i\{(1 - b_i)^2\Gamma_{0k} + (3b_i / 2 - b_i^2)\Gamma_{1k}\} + 3\zeta_i(1 + \zeta_i Z_i)\Gamma_{0k} - \{\zeta_i + 2\zeta_i^3(1 + \zeta_i Z_i)\}\Gamma_{0k}]$

and

$L = 2\zeta_e(1 - \omega_* / \omega)[Z_e + \zeta_e(1 + \zeta_e Z_e)]$

$- \eta_e \zeta_e \omega_* / \omega\,[Z_e + \zeta_e(1 + \zeta_e Z_e) + \zeta_e\{(1 + 2\,\zeta_e^2(1 + \zeta_e Z_e)\}]$.

3.2 Result of Nonlinear Simulation

Figure 5 shows (a) the frequency and (b) the growth rate of linear mode with $k_x\rho_i = 0.1$ and $k_{//}\rho_i = 0.01$. The solid curve represents the case with $\eta_i = 3$, $\eta_e = 3$ and the dashed curve the case with $\eta_i = 3$, $\eta_e = 0$. The destabilization mechanism for short wavelength ITG mode comes from the finite Larmor radius(FLR) effect and the electron temperature gradient further enhances the instability[3].

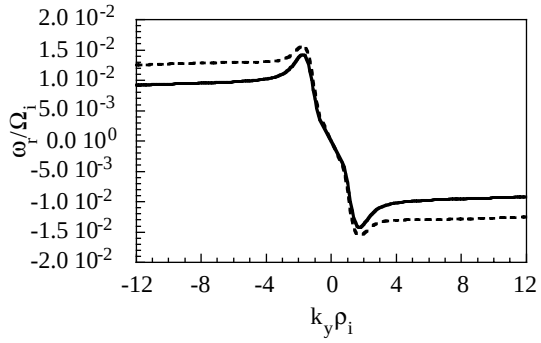

FIG.5 (a) the frequency of linear mode.

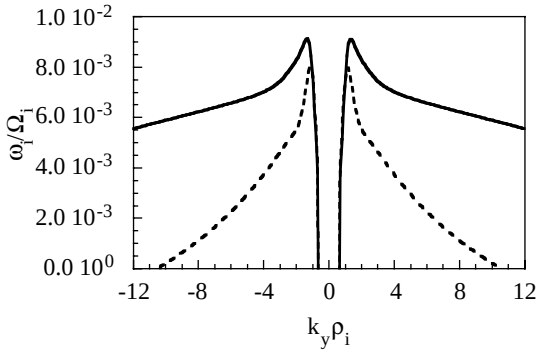

FIG5(b) the growth rate of linear mode.

The nonlinear simulation is performed using the spectral code. The minimum wavenumbers are $k_{x0}\rho_i = 0.1$, $k_{y0}\rho_i = 0.1$, $k_{z0}\rho_i = 0.01$, respectively and $8 \times 128 \times 16$ Fourier modes are used. Other parameters are given by $\tau = 1$, $m_i / m_e = 1836$, $\rho_i / L_n = 0.2$, $\Omega_i^2 / \omega_{pi}^2 = 10$. Initially, the linear frequency and growth rate are evaluated, then ω in eqs. (5) and (6) is fixed as a parameter, therefore, we regard eqs.(5) and (6) as the coupled first order ordinary differential equations. The nonlinear Landau damping is not taken into account in this numerical scheme. Figure 6 shows the time evolution of the drift wave energy and the convective cell energy defined by eq.(7). The solid curve represents the drift wave energy and the dashed curve the convective cell energy. Figure 7 shows the time evolution of 1D spectrum of the potential energy. Time slices at $\Omega_i t = 100,200,300,350$ are plotted. The cascade in $k_{//}$ space is observed and the convective cell is excited by the nonlinear interaction.

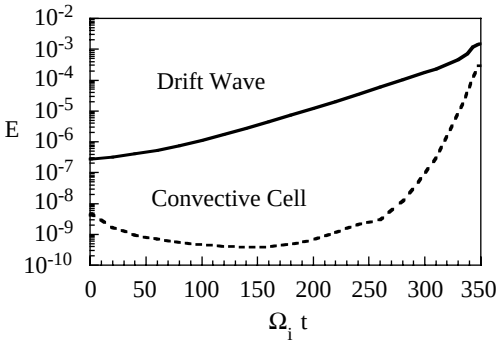

FIG.6 Time evolution of the drift energy and the convective cell energy.

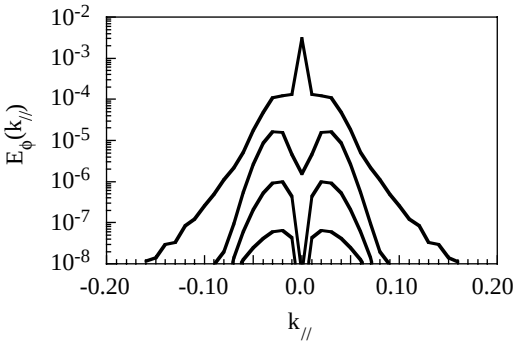

FIG.7 Time evolution of 1D spectrum of potential energy.

Figure 8 shows the time evolution of 2D spectra of the potential energy in the case with $k_x\rho_i = 0.3$. Time slices at $\Omega_i t = 100,200,300,350$ are plotted. The inverse cascade occurs in the longest wavelength region. The another peak appears in the short wavelength region.

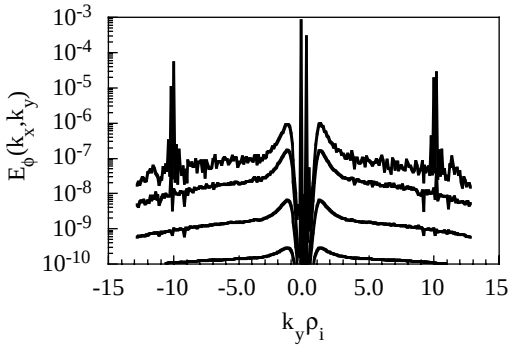

FIG.8 Time evolution of 2D spectrum of potential energy.

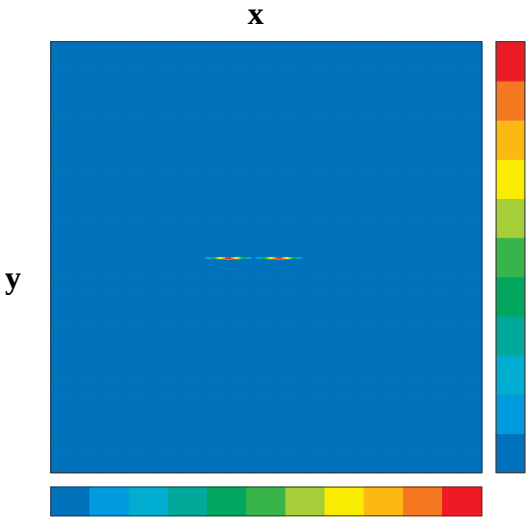

FIG. 9 Contour plot of potential at $t = 350$.

Figure 9 shows the contour plot of the electrostatic potential $\phi(x,y,z=0)$ at $t = 350$. Two vortex elongated in the x direction are observed, which corresponds to 'streamers'. However, the single elongated vortex in the x direction is observed in the contour plot of flux around $x = 0, y = 0$. It is found that $\Gamma_{n0} < 0$ (corresponding to the averaged particle flux) for $\eta_e = 3$, on the other hand, $\Gamma_{n0} > 0$ for $\eta_e = 0$, which means particle pinch occurs in the case with $\eta_e = 3$. For electron and ion heat flux, they have positive values for both cases. This result indicates the nonlinear interaction between different scale length mode might affect transport.

4. Summary and Discussion

In this paper, nonlinear interactions of fluctuations with different scale lengths are investigated. First is the theoretical approach: the hierarchical model for multiple-scale turbulence is developed and a set of Langevin equations is formulated. Using this model, a case where two driving mechanism coexist is investigated. It is found that (1) a new type of turbulence transition and a cusp-type catastrophe exist in the case without the noise effect due to the micro mode. Next, assuming Gaussian white noise, the Fokker-Planck equation is derived to

investigate the noise effect on multiple-scale turbulence. It is shown that (2) the noise effect change the phase diagram drastically. More detailed study on the noise character should be necessary and it is left for future work. The second approach is the numerical simulation to investigate cascade and inverse cascade in multiple-scale turbulence. ITG and short wavelength ITG mode in the shearless slab geometry are considered as a first step. It is found that (3) the cascade occurs in $k_{//}$ space, on the other hand, both the cascade and inverse cascade occur in $k_{\perp}$ space. Another interesting result is that (4) the particle flux has a negative value in the case with $\eta_e = 3$, although it has a positive value in the case with $\eta_e = 0$. More quantitative analysis should be necessary and it is left for future work.

Acknowledgements:
One of the authors (MY) acknowledges Dr. C. Z. Cheng and Dr. A. Smolyakov for useful discussions. This work is partly supported by the Grant-in-Aid for Scientific Research of MEXT Japan, by the collaboration programmes of National Institute for Fusion Science, of the Research Institute for Applied Mechanics of Kyushu University and of US-Japan Joint Interchange Fusion Theory and by Asada Eiichi Research Foundation.

References:
[1] ITOH, K., ITOH, S.-I. and FUKUYAMA, A., *Transport and Structural Formation in Plasmas* (IOP, Bristol, 1999)
[2] DIAMOND, P. H. et al., 17th IAEA Fusion Energy Conference, Yokohama, Japan, (1998) TH3/1.
[3] SMOLYAKOV, A., YAGI, M. and KISHIMOTO, Y., Phys. Rev. Lett. **89** (2002) 125005 and 19th IAEA Fusion Energy Conference, Lyon, France, (2002) TH/P1-14.
[4] ITOH, K., YAGI, M., ITOH, S.-I., FUKUYAMA, A. and AZUMI, M., Plasma Phys. Control. Fusion **35** (1993) 543.
[5] ITOH, S.-I. and ITOH, K., Plasma Phys. Control. Fusion **43** (2001) 1055.
[6] KAWASAKI, M., ITOH, S.-I. and ITOH, K., to be published.
[7] CHENG, C. Z. and JOHNSON, J. R., J. Geophys. Res. **104** (1999) 413.
[8] ANTONSEN, T. and LANE, B., Phys. Fluids **23** (1980) 1205.